0022-3565/06/3191-8–19$20.00
THE JOURNAL OF PHARMACOLOGY AND EXPERIMENTAL THERAPEUTICS
JPET 319:8–19, 2006

Vol. 319, No. 1
106054/3137852
Printed in U.S.A.

Intracellular Delivery of the p38 Mitogen-Activated Protein Kinase Inhibitor SB202190 [4-(4-Fluorophenyl)-2-(4-hydroxyphenyl)-5-(4-pyridyl)1*H*-imidazole] in Renal Tubular Cells: A Novel Strategy to Treat Renal Fibrosis

Jai Prakash, Maria Sandovici, Vinay Saluja, Marie Lacombe, Roel Q. J. Schaapveld, Martin H. de Borst, Harry van Goor, Robert H. Henning, Johannes H. Proost, Frits Moolenaar, György Këri, Dirk K. F. Meijer, Klaas Poelstra, and Robbert J. Kok

Departments of Pharmacokinetics and Drug Delivery (J.P., V.S., J.H.P., F.M., D.K.F.M, K.P., R.J.K.), Clinical Pharmacology (M.S., R.H.H.), and Pathology and Laboratory Medicine (M.H.d.B., H.v.G.), Groningen University Institute for Drug Exploration, Groningen, The Netherlands; Kreatech Biotechnology B.V., Amsterdam, The Netherlands (M.L., R.Q.J.S.); Vichem Chemie Research Ltd., Budapest, Hungary (G.K.); and Department of Pharmaceutics, Utrecht University, Utrecht, The Netherlands (R.J.K.)

Received April 12, 2006; accepted June 27, 2006

ABSTRACT

During renal injury, activation of p38 mitogen-activated protein kinase (MAPK) in proximal tubular cells plays an important role in the inflammatory events that eventually lead to renal fibrosis. We hypothesized that local inhibition of p38 within these cells may be an interesting approach for the treatment of renal fibrosis. To effectuate this, we developed a renal-specific conjugate of the p38 inhibitor SB202190 [4-(4-fluorophenyl)-2-(4-hydroxyphenyl)-5-(4-pyridyl)1*H*-imidazole] and the carrier lysozyme. First, we demonstrated that SB202190 inhibited the expression of albumin-induced proinflammatory (monocyte chemoattractant protein-1) and transforming growth factor (TGF)-β1-induced profibrotic (procollagen-Iα1) genes over 50% in renal tubular cells (normal rat kidney-52E). Next, we conjugated SB202190 via a carbamate linkage to lysozyme. However, this conjugate rapidly released the drug upon incubation in serum. Therefore, we applied a new platinum(II)-based linker approach, the so-called universal linkage system (ULS), which forms a coordinative bond with SB202190. The SB202190-ULS-lysozyme remained stable in serum but released the drug in kidney homogenates. SB202190-ULS-lysozyme accumulated efficiently in renal tubular cells and provided a local drug reservoir during a period of 3 days after a single intravenous injection. Treatment with SB202190-ULS-lysozyme inhibited TGF-β1-induced gene expression for procollagen-Iα1 by 64% in HK-2 cells. Lastly, we evaluated the efficacy of a single dose of the conjugate in the unilateral renal ischemia-reperfusion rat model. A reduction of intrarenal p38 phosphorylation and α-smooth muscle actin protein expression was observed 4 days after the ischemia-reperfusion injury. In conclusion, we have developed a novel strategy for local delivery of the p38 MAPK inhibitor SB202190, which may be of use in the treatment of renal fibrosis.

Efficient treatment of renal fibrosis is one of the major challenges in the field of nephrology because there is a trend of a continuously increasing number of patients each year worldwide (Meguid El and Bello, 2005). Current therapies, such as inhibition of renin-angiotensin system components, have yet not been able to prevent end-stage renal diseases; therefore, more specific approaches are required. It has been described that renal tubular cells play a pivotal role in the initiation of inflammatory processes leading to interstitial fibrosis (Strutz, 2001). During a renal insult, tubular cells are activated by various stimuli such as filtered proteins, cytokines, or hypoxia, upon which they produce several proinflammatory chemotactic factors [e.g., monocyte che-

Part of this work was presented: Prakash J, Poelstra K, Moolenaar F, and Kok RK (2005) A new strategy to treat renal fibrosis: targeting of p30 MAPK inhibitor SB202190 to the kidney, *3rd World Congress of Nephrology*; 2005 Jun 26–30; Singapore, Singapore. World Congress of Nephrology, Brussels, Belgium; and Prakash J, Saluja V, Poelstra K, Meijer DKF, Moolenaar F, and Kok RJ (2005) Renal targeting of p38 MAPK inhibitor SB202190 to treat renal fibrosis, *Renal Week of the American Society for Nephrology*; 2005 Nov 8–13; Philadelphia, PA. American Society of Nephrology, Washington, DC.

Article, publication date, and citation information can be found at http://jpet.aspetjournals.org.

doi:10.1124/jpet.106.106054.

ABBREVIATIONS: MCP, monocyte chemoattractant protein; TGF, transforming growth factor; MAPK, mitogen-activated protein kinase; LZM, lysozyme; SB202190, 4-(4-fluorophenyl)-2-(4-hydroxyphenyl)-5-(4-pyridyl)1*H*-imidazole; ULS, universal linkage system; SB, SB202190; NRK, normal rat kidney; RT, reverse transcription; PCR, polymerase chain reaction; TIMP, tissue inhibitor of metalloproteinase; NSED, *N*-succinimidyl-*N*-boc-ethylenediamine; ESI, electrospray ionization; MS, mass spectrometry; HPLC, high-performance liquid chromatography; DMF, dimethylformamide; PBS, phosphate-buffered saline; GSH, glutathione; TUNEL, terminal deoxynucleotidyl transferase dUTP nick-end labeling; i.v., intravenous; I/R, ischemia-reperfusion; BSA, bovine serum albumin; SMA, smooth muscle action.

moattractant protein (MCP)-1 and chemokine (C-C motif) ligand 5] and profibrotic factors (TGF-β1) (Zoja et al., 1998; Morigi et al., 2002; Takaya et al., 2003; Wolf et al., 2004). These factors further activate tubular cells, macrophages, and fibroblasts. p38 mitogen-activated protein kinase (MAPK) plays a crucial role in the activation of tubular cells and in the secretion of various cytokines from tubular cells (de Borst et al., 2005). Therefore, blockade of p38 in tubular cells may be valuable for the treatment of renal injuries. The beneficial role of p38 inhibitors has been demonstrated for the treatment of renal injuries (Stambe et al., 2004; Koshikawa et al., 2005). However, tubular cell-specific effects were not delineated, and relatively high doses were required to achieve a therapeutic effect. Moreover, several clinical trials showed that p38 inhibitors exerted various side effects in other organs, such as immunosuppression, as reviewed (Kumar et al., 2003). Such a systemic immunosuppressive effect of a drug against renal fibrosis is unfavorable. Therefore, we hypothesized that renal-specific drug delivery can greatly improve the therapeutic profile of p38 MAPK inhibitors for renal disorders.

Target cell-specific drug delivery is an attractive approach to investigate the cell-specific effects of drugs because it can avoid interactions with nontargeted cells in other organs and thereby decrease side effects. Furthermore, drug delivery can augment local drugs levels at the target site, thereby improving therapeutic efficacy. We have gathered unique expertise in delivering the drugs to the kidneys using the low-mol. wt. protein lysozyme (LZM) as drug carrier (Haas et al., 2002). We now propose to use drug-LZM conjugates for the delivery of antifibrotic kinase inhibitors. Recently, we evaluated the pharmacokinetics of the well-known p38 inhibitor SB202190 and demonstrated that it distributed poorly to the kidneys (Prakash et al., 2005a). This result underscored the need for drug delivery of this type of hydrophobic compounds to achieve appropriate drug levels in the kidney, which predominantly accumulates hydrophilic compounds.

Although SB202190 has been used extensively as model compound for p38 inhibition, only a few studies report its use in renal tubular cells, e.g., after activating them with angiotensin II and insulin (Bhaskaran et al., 2003; Harrison et al., 2006). In these studies, SB202190 reduced angiotensin II-induced apoptosis in tubular cells but did not alter the effect of insulin in these cells. In the present study, therefore, we first evaluated the effect of SB202190 on fibrotic signaling cascades in renal tubular cells. Furthermore, we conjugated SB202190 to LZM via two different strategies: We conjugated the drug via a carbamate linkage, which appeared suitable for the hydroxyl group of SB202190; and we employed a new platinum-based linkage system called universal linkage system (ULS) to couple the drug via a coordinative bond at its pyridinyl group. The latter coupling strategy offers advantages with respect to the synthesis and stability of the constructs. Because platinum compounds are known to produce nephrotoxicity (Wolfgang et al., 1994; Park et al., 2002), we investigated the SB202190-ULS-LZM conjugate (further referred to as SB-ULS-LZM) for cytotoxicity in renal tubular cells in cell cultures and in vivo. In addition, we investigated the drug release profile of the SB-LZM conjugates in vitro and evaluated the pharmacokinetics of SB-ULS-LZM in normal rats. Lastly, we tested the capability of SB-ULS-LZM to interfere with fibrotic signaling events in human renal tubular cells in vitro and in the unilateral ischemia-reperfusion renal injury model in vivo in rats.

Materials and Methods

Cells and Animals

Normal rat kidney (NRK)-52E cells were kindly provided by Prof. Russel (University of Nijmegen, Nijmegen, The Netherlands). Cells were cultured in Dulbecco's modified Eagle's medium (BioWhittaker, Verviers, Belgium) supplemented with 5% fetal calf serum (BioWhittaker), 4 mM L-glutamine, 50 units/ml penicillin, and 50 ng/ml streptomycin. Human kidney tubular cells (HK-2) were obtained from ATCC (Manassas, VA) and grown in RPMI 1640 medium supplemented with 10% fetal calf serum, 2 mM L-glutamine, 100 units/ml penicillin, and 100 ng/ml streptomycin. Human recombinant TGF-β1 was purchased from Roche Diagnostics (Mannheim, Germany).

All experimental protocols for animal studies were approved by the Animal Ethics Committee of the University of Groningen. Normal male Wistar rats (220–240 g) were obtained from Harlan (Zeist, The Netherlands).

Determination of mRNA Expression

After the treatments (as described in the legends of the figures), cells were harvested using lysis buffer, and total RNA was isolated from the cells using the Stratagene Microkit (Stratagene, La Jolla, CA). RNA content was measured by a nanodrop UV detector (NanoDrop Technologies, Wilmington, DE). cDNA was synthesized from similar amounts of RNA using the Superscript III first-strand synthesis kit (Invitrogen, Carlsbad, CA). Gene expression levels for the following genes were measured by quantitative real-time RT-PCR (Applied Biosystems, Foster City, CA). The primers for rat species were obtained from Sigma-Genosys (Haverhill, UK) as follows: MCP-1, 5′-TCCTCCACCACTATGCAGGT-3′ and 5′-TTCCTTATTGGGGTCAGCAC-3′, 255 bp; tissue inhibitor of metalloproteinase (TIMP)-1, 5′-GAGAGCCTCTGTGGATATGT-3′ and 5′-CAGCCAGCACTATAGGTCTT-3′, 334 bp; procollagen-Iα1, 5′-AGCCTGAGCCAGCAGATTGA-3′ and 5′-CCAGGTTGCAGCCTTGGTTA-3′, 145 bp; and glyceraldehyde-3-phosphate dehydrogenase, 5′-CGCTGGTGCTGAGTATGTCG-3′ and 5′-CTGTGGTCATGAGCCCTTCC-3′, 179 bp. The TaqMan primers for Human species were obtained from Applied Biosystems (Assay-On-Demand; Warrington, UK).

For NRK-52E cells, SYBR Green PCR Master Mix (Applied Biosystems) was used as a fluorescent probe for real-time RT-PCR. For each sample, 1 μl of cDNA was mixed with 0.4 μl of each gene-specific primer (50 μM), 0.8 μl dimethyl sulfoxide, 8.4 μl of water, and 10 μl of SYBR Green PCR Master Mix. For HK-2 cells, qPCR Mastermix Plus (Eurogentec, Seraing, Belgium) was used as a fluorescent probe for real-time RT-PCR. For each sample, 1.25 μl of cDNA was mixed with 0.5 μl of each gene-specific primer, 4.5 μl of water, and 5 μl of qPCR Mastermix Plus. The cDNA amplification was performed until 40 cycles. Finally, the threshold cycle number was calculated for each gene, and relative gene expressions were calculated after normalizing for the expression of the control gene glyceraldehyde-3-phosphate dehydrogenase.

Synthesis of SB-Carbamate-LZM

SB201290 (3 μmol; L.C. Laboratories, Woburn, MA) was reacted with *N*-succinimidyl-*N*-boc-ethylenediamine (NSED; 90 μmol; Sigma, St. Louis, MO) in dichloromethane in the presence of tributylamine (60 μmol) with stirring for 24 h at room temperature. After completion of the reaction, as demonstrated by thin-layer chromatography [silica plates, ethyl acetate/acetone, 1:1 (v/v)], the intermediate product was purified on preparative silica thin layer chromatography and characterized by electrospray ionization (ESI)-mass spectrometry (MS) and HPLC analysis. The boc group was removed by incubating with 10% trifluoroacetic acid for 1 h. After evaporation of the acid under reduced pressure, the deprotected amine (3 μmol)

was then reacted with γ-maleimidobutyryloxysuccinimide ester (2.7 μmol; Sigma) in dimethylformamide (DMF) and dichloromethane (1:1) for 1 h in the presence of tributylamine (42 μmol). The product was evaluated by ESI-MS and HPLC analysis. Total amount of SB202190-carbamate product was calculated by estimating SB202190 with HPLC analysis by detaching it in strong basic condition.

To introduce thiol groups that can be reacted with the maleimidyl group of the SB202190-carbamate adduct, egg white LZM (1.4 μmol; Sigma) was modified with *N*-succinimidyl-*S*-acetylthioacetate (2.1 μmol; Sigma) in 0.1 M phosphate-buffered saline (PBS) for 1 h. The product was dialyzed against PBS, pH 7.4, for 24 h, and the purified product was treated with 0.1 M hydroxylamine and EDTA (25 mM) to deprotect the thiol group. The SB202190-carbamate product (2.8 μmol) dissolved in DMF was slowly added to the solution of LZM-SH (1.4 μmol) in PBS, pH 7.4, and reacted for 2 h at room temperature. The final product was dialyzed against water, filtered with a 0.2-μm syringe filter, lyophilized, and stored at −20°C. The conjugate was characterized by ESI-MS analysis for the whole conjugate and by HPLC analysis for SB202190, as described earlier (Prakash et al., 2005a). For this latter analysis, the coupled drug was released by incubating with 0.5 M NaOH at 37°C for 24 h.

Synthesis of SB-ULS-LZM

Synthesis of SB202190-ULS. SB202190 was coupled with ULS in 1:1 mol/mol ratio. *cis*-[Pt(ethylenediamine)nitrate-chloride] (ULS; 5.2 μmol) was added to SB202190 (5.4 μmol, 10 mg/ml in DMF) and heated at 37°C for 3 h. The reaction mixture then was evaporated to dryness under reduced pressure, affording a pale yellow solid (yield, 92%) that was analyzed by HPLC, ^{1}H NMR, and ESI-MS. These analyses confirmed the 1:1 coupling ratio of drug and linker: ^{1}H NMR of free SB202190 (CD_3OD): δ_H 6.88 (d, J = 8.74 Hz, 2*H*, *F*$(CHCH)_2$), 7.17 (m, 2*H*, N$(CHCH)_2$), 7.50 (m, 4*H*, $(CHCH)_2$OH), 7.82 (d, J = 8.68 Hz, 2*H*, *F*$(CHCH)_2$), 8.41 (m, 2*H*, N$(CHCH)_2$) ppm; ^{1}H NMR of SB202190-ULS (CD_3OD): δ_H 2.59 (m, 4*H*, $H_2N(CH_2)_2NH_2$), 5.58 (s, 2*H*, NH_2), 5.91 (s, 2*H*, NH_2), 6.89 (d, J = 8.75 Hz, 2*H*, *F*$(CHCH)_2$), 7.22 (m, 2*H*, N$(CHCH)_2$), 7.53 (m, 4*H*, $(CHCH)_2$OH), 7.82 (d, J = 8.73 Hz, 2*H*, *F*$(CHCH)_2$), 8.52 (m, 2*H*, N$(CHCH)_2$) ppm; MS (ESI$^+$) *m/z*: 622 [M +H]$^+$, 585 [M-Cl$^-$-H$^+$]$^+$.

Synthesis of SB-ULS-LZM. Drug-ULS adducts react readily with thiol groups of methionine and cysteine residues at 37°C, as has been demonstrated with albumin carrier proteins (Gonzalo et al., 2006). Pilot experiment showed that LZM did not react readily with fluorescein-ULS (data not shown), presumably because the methionine residues and disulfide bridges are buried in the core of the protein. Therefore, we introduced additional methionine residues onto the protein surface by chemical derivatization of lysyl residues. Boc-L-methionine hydroxysuccinimide ester (0.84 μmol; Fluka, Buchs, Switzerland) was dissolved in dimethyl sulfoxide and added to LZM (0.7 μmol, 10 mg/ml in 0.1 M sodium bicarbonate buffer, pH 8.5). The mixture was stirred for 1 h at room temperature. The product was dialyzed against water for 48 h, filtered through a 0.2-μm membrane filter, lyophilized, and characterized by ESI-MS analysis. Methionine-LZM was further reacted with SB202190-ULS to obtain the final SB-ULS-LZM conjugate. SB202190-ULS (2.1 μmol) in DMF was added to methionine-LZM (0.7 μmol) dissolved in ULS labeling buffer (20 mM Tricine/$NaNO_3$ buffer, pH 8.5). The mixture was reacted at 37°C for 24 h, after which the product was dialyzed against water for 48 h, filtered, lyophilized, and stored at −20°C. ESI-MS and HPLC analyses of the coupled SB202190 were performed to confirm the composition of the SB-ULS-LZM conjugate. The conjugated drug was determined after releasing the drug from the SB-ULS-LZM conjugate by competitive displacement with an excess of thiocyanate, which is an excellent ligand for platinum coordination. In brief, appropriate aliquots of the conjugate (0.2 mg/ml in PBS) were incubated with 0.5 M potassium thiocyanate in PBS at 80°C for 24. The released SB202190 was estimated by HPLC as described before (Prakash et al., 2005a). Free drug levels in the preparation were also investigated by HPLC analysis of freshly prepared appropriate dilutions of the conjugate in PBS.

Stability of the Conjugates

Drug-free serum and kidneys were obtained from healthy male Wistar rats. Kidney homogenates were prepared in PBS, pH 7.4, or sodium acetate buffer, pH 5.0, in 1:3 (w/v) using an Ultra-Turrax-T25 apparatus (IKA; Stauffen, Germany) at the highest speed. All matrices were kept on ice before incubation with the conjugate. SB-carbamate-LZM was incubated with PBS, serum, and kidney homogenates, pH 7.4 and 5.0, whereas SB-ULS-LZM was incubated in the conditions listed above and in 0.1 M sodium acetate buffer, pH 5.0, and 5 mM glutathione (GSH) in PBS. Incubations were performed at 37°C, and 100-μl aliquots were taken at 2, 6, and 24 h, after which they were processed immediately for HPLC analysis of SB202190.

Assessment of the Toxicity of ULS Conjugates

We determined the platinum-related cellular toxicity of the SB-ULS adduct and its lysozyme conjugate in the renal tubular cell line NRK-52E. Cells were seeded at 10^4 cells/well in 96-well plates in culture medium (200 μl). After 24 h of incubation, medium was replaced by medium containing different dilutions of cisplatin or the ULS-containing compounds. Plates were incubated for 24 h, after which cell viability was assessed by Alamar Blue assay (Serotec, Oxford, UK).

Pharmacokinetics of SB-ULS-LZM

Rats (n = 11) were injected with a single dose of the SB-ULS-LZM conjugate (16 mg/kg equivalent to 376 μg/kg SB202190, dissolved in 5% glucose) that was administered i.v. through the penile vein under inhalation anesthesia. Animals were placed back into metabolic cages to collect urine, which was combined with urine collected from the urinary bladder after sacrificing the animals. At each indicated time point, with the exception of 24 h (n = 2), a single animal was sacrificed. This procedure was chosen to characterize the pharmacokinetics of the compounds, allowing multicompartmental curve fitting (see below). At 5 and 15 min and 1, 2, 6, 12, 24, 36, 48, and 72 h, animals were anesthetized, blood samples were collected by heart puncture, and kidneys were isolated after gently flushing the organs with saline. Kidneys were weighed, and half of the kidney was homogenized [1:3 (w/v) PBS], which was stored at −80°C. Released drug amounts were estimated by HPLC analysis after extraction as described above. To estimate total drug (bound plus released), samples were treated with potassium thiocyanate to release SB202190 from the ULS linker as described above and then subjected to HPLC analysis. Anti-LZM immunohistochemical staining was performed on frozen kidney sections to detect the renal uptake of the conjugate.

In vivo toxicity of ULS after administration of SB-ULS-LZM was assessed in the same animals as used for the pharmacokinetic study and compared with untreated animals (n = 4) and to the animals treated with a dose of cisplatin (3 mg/kg i.v., n = 4) for 24 h. This dose of cisplatin is 8-fold higher than the amount of platinum in the SB-ULS-LZM conjugate. To examine the effect on the renal function, serum and urine creatinine levels were determined to calculate creatinine clearance. In the case of SB-ULS-LZM-treated animals, creatinine clearance at 24, 32, 48, and 72 h was calculated from serum and urine samples collected at the latest 24 h before sacrificing the animals. To calculate proteinuria for the SB-ULS-LZM group, the mean of the urinary protein levels at different days was taken. TUNEL staining and Masson staining were performed on kidney cryostat sections to examine the number of apoptotic cells and changes in renal morphology. In addition, we determined the platinum levels in kidneys using inductively coupled plasma-atomic absorption spectrometry after digestion of the tissue in concentrated nitric acid for 24 h at room temperature and heating at 70°C until the formation of clear solution.

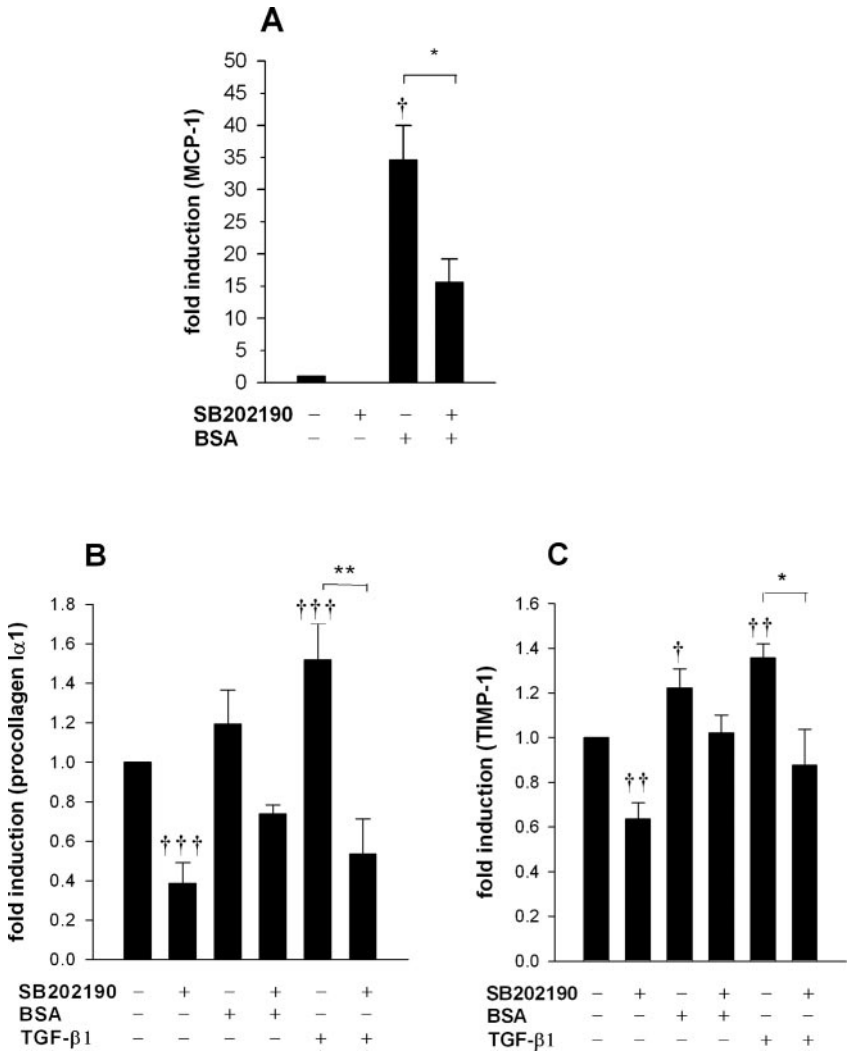

Fig. 1. Effects of SB202190 on albumin- or TGF-β1-induced gene expressions of MCP-1 (A), procollagen-Iα1 (B), and TIMP-1 (C) in NRK-52E cells. Cells were grown to 80% confluence in 12-well plates and then deprived from serum for 24 h. Thereafter the cells were preincubated for 2 h with SB202190 (10 μM) and then activated with either BSA (30 mg/ml) or TGF-β1 (10 ng/ml) for 24 h. After that, cells were harvested for RNA isolation. The mRNA expressions were determined by quantitative RT-PCR. Data represent the mean $\pm$ S.E.M. for at least three independent experiments. Differences versus control are presented as: †, $p < 0.05$; ††, $p < 0.01$; and †††, $p < 0.001$. Other differences are: *, $p < 0.05$; **, $p < 0.01$; and ***, $p < 0.001$.

Efficacy of SB-ULS-LZM in Unilateral Ischemia-Reperfusion Rats

The pharmacological efficacy of SB-ULS-LZM was evaluated in the unilateral ischemia-reperfusion (I/R) rat model. At 2 h before the ischemia procedure, rats were injected with SB-ULS-LZM (32 mg/kg conjugate, equivalent to 752 μg/kg SB202190; $n = 6$), vehicle (5% glucose; $n = 6$), or free SB202190 (800 μg/kg; $n = 3$). SB-ULS-LZM was dissolved in 5% glucose, whereas SB202190 was dissolved in 20% hydroxypropyl-β-cyclodextrin solution with 5% dimethyl sulfoxide as described earlier (Prakash et al., 2005a). Compounds were administered i.v. via the penis vein as described above. Animals were allowed to recover and placed back into the cages until the induction of renal ischemia. Rats were operated, and the renal artery and vein were clamped under microscope to stop renal blood flow. After 45 min, clamps were removed, and reperfusion of the kidney was observed before closing of the wound. Sham-operated animals ($n = 3$) received the same surgical procedure, with the exception of ischemia, and were included as a control group. After 4 days, animals were sacrificed, and blood samples were collected from the abdominal aorta. Kidneys were isolated after gently flushing the organs with saline and preserved in 4% formalin for preparation of paraffin-embedded sections or frozen in ice-cold isopentane for preparation of cryosections.

Histological and Immunohistochemical Analyses

Kidney cryostat sections were used for immunohistochemical detection of LZM, α-SMA, and TUNEL-positive cells and for Masson staining. Cryostat sections of 4-μm thickness were fixed with acetone and incubated with rabbit anti-LZM polyclonal IgG (dilution 1:500; Chemicon, Temecula, CA) or anti-α-SMA monoclonal IgG (dilution 1:500; Sigma) for 1 h at room temperature. After washing with PBS, sections were incubated with hydrogen peroxide (0.07% in PBS) to inactivate endogenous peroxidase activity and subsequently incubated with goat anti-rabbit or rabbit anti-mouse horseradish peroxide-conjugated antibodies (dilution, 1:50; DakoCytomation Denmark A/S, Glostrup, Denmark) for 20 min. Peroxidase activity was visualized with 3-amino-9-ethylcarbazole as red color. Sections were counter-stained with hematoxylin and mounted with Kaiser's glycerin gelatin solution. TUNEL staining (TUNEL Pod Kit, Roche Diagnostics) was performed according to the supplier's protocol. Positively stained cells were counted in 10 different fields (magnification, 200$\times$) of kidney cortex region using NIH Image J software. Masson staining was performed according to standard protocols.

Anti-p-p38 immunohistochemical staining was performed on 3-μm-thick paraffin-embedded sections. Sections were deparaffinized in xylene and rehydrated in alcohol and distilled water. To retrieve antigen, sections were boiled in 10 mM citrate buffer, pH 6.0, for 10 min in microwave and cooled down. Then, sections were incubated with 3% hydrogen peroxide for 10 min. After washing in distilled water, sections were blocked with 1% bovine serum albumin (BSA) for 1 h and incubated with rabbit anti-p-p38 monoclonal IgG (dilution, 1:100; Cell Signaling, Danvers, MA) overnight at 4°C. After washing three times with Tris-buffered saline, pH 7.6, sections were incubated with secondary goat-anti-rabbit antibody and subse-

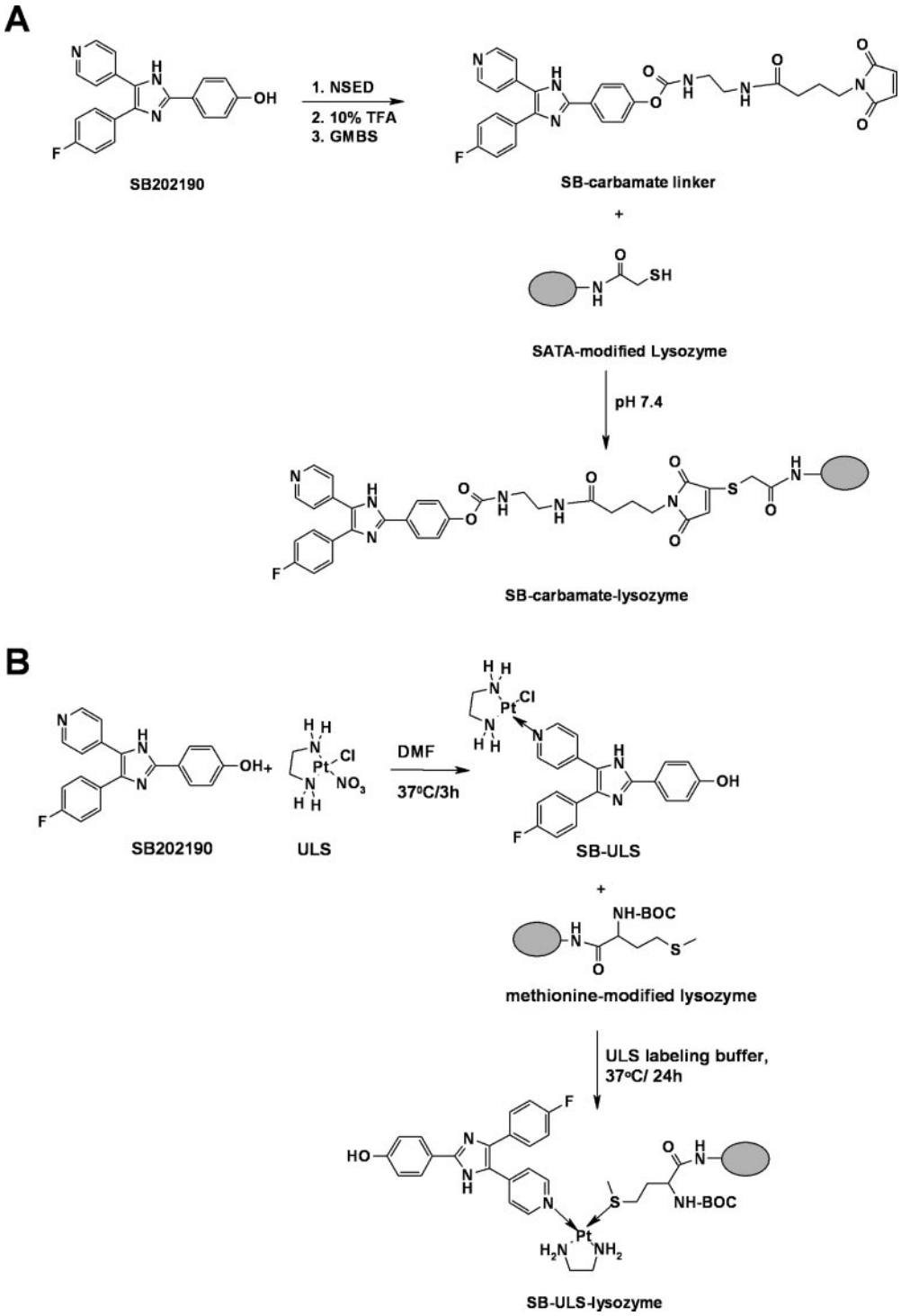

Fig. 2. Synthesis scheme of SB-carbamate-LZM (A) and SB-ULS-LZM conjugates (B). Large filled circles, LZM. TFA, trifluoroacetic acid; GMBS, γ-maleimidobutyryloxysuccinimide ester; SATA, *N*-succinimidyl-*S*-acetylthioacetate.

quently with rabbit-anti-goat hydrogen peroxidase (DakoCytomation Denmark A/S) each for 20 min. Finally, staining was developed with 3,3′diaminobenzidine tetrahydrochloride.

Semi quantification of α-SMA and p-p38 immunohistochemical staining was performed by two independent observer in a double-blind manner. Each section was scored as following: −, negative; −/+, faint staining; +, occasional positive; ++, strong; and +++, abundant staining.

Statistical Analysis

The statistical analyses were performed using Student's t test with $p < 0.05$ as the minimal level of significance. Results are presented as mean ± S.E.M. Pharmacokinetic analysis of the plasma SB202190 concentrations was performed using the Multifit program (Department of Pharmacokinetics and Drug Delivery, University of Groningen).

Results

Effect of SB202190 on Fibrotic Signaling in Renal Tubular Cells

To investigate the effect of SB202190 on proinflammatory and profibrotic signaling cascades in renal tubular cells, we

activated NRK-52E cells with either 30 mg/ml BSA or 10 ng/ml TGF-β1. Albumin stimulated the gene expression of the inflammation marker MCP-1 over 30-fold, which in turn could be reduced by 55% after p38 inhibition (Fig. 1A). Furthermore, BSA enhanced the gene expressions of TIMP-1 significantly, whereas procollagen-Iα1 was not elevated significantly (Fig. 1, B and C). Treatment with SB202190 reduced the expression of these genes to levels below basal expression, as was also observed for nonactivated cells that were treated with the drug. Similarly TGF-β1 also induced the gene expression of procollagen-Iα1 and TIMP-1 significantly in 24 h, and treatment with SB202190 inhibited the gene expression of all the genes significantly (Fig. 1, B and C). MCP-1 expression was not effected by TGF-β1 treatment (data not shown).

Synthesis and Characterization of SB202190-LZM Conjugates

SB-Carbamate-LZM Conjugate (Fig. 2A). SB202190 was converted to SB202190-NSED with an overall yield of 88% after purification, as estimated by HPLC analysis. Next, SB202190-NSED was reacted with γ-maleimidobutyryloxy-succinimide ester and provided the SB202190-carbamate linker adduct at 90% yield. SB202190-carbamate was reacted to thiol-modified LZM, which produced a SB-carbamate-LZM conjugate with an average drug/carrier ratio of 0.7:1, as characterized by mass spectrometry of the whole conjugate and by HPLC analysis of the coupled drug.

SB-ULS-LZM Conjugate (Fig. 2B). SB202190 was efficiently coupled with ULS yielding the drug-ULS 1:1 adduct at an overall yield of 92%. The identity of the product was confirmed by HPLC, ^{1}H NMR, and ESI-MS. ^{1}H NMR and Pt-NMR studies indicated that SB202190 was coordinated to ULS at the pyridinyl nitrogen of the drug. The resulting methionine-LZM carrier was straightforwardly converted in the SB-ULS-LZM product by incubating with drug-ULS overnight. The final product was characterized by mass spectrometry of the whole conjugate and by HPLC analysis of the coupled drug, confirming 1:1 drug to protein coupling.

In an ideal drug delivery conjugate, the drug-carrier linkage should be stable during storage and in the systemic circulation to reach the target cells intactly. In addition, the linkage should display an appropriate drug-release profile once the conjugate has been accumulated in target cells to provide the pharmacologically active compound. Figure 3, A and B, show the drug-release profile of the SB-carbamate-LZM and SB-ULS-LZM conjugates, respectively. A clear difference was observed in the stability of the two types of conjugates. SB-carbamate-LZM was unstable in PBS and even more unstable in serum, whereas SB-ULS-LZM conjugate remained stable in both media. In kidney homogenate, the target tissue of the constructs, both conjugates displayed gradual release of the drug at pH 7.4, but at pH 5.0, only SB-ULS-LZM did release the drug (Fig. 3, A and B). Because the constructs are taken up via endocytosis and drug release should occur in lysosomes, pH 5.0, this is quite relevant. In vivo, endogenous compounds such as GSH can bind to platinum and thereby displace the drug. We found that SB-ULS-LZM released the drug maximally at 2 h after incubating with GSH, and no further release occurred until 24 h. Based on the release profile in serum and kidney homogenates, we decided to pursue our study with SB-ULS-LZM.

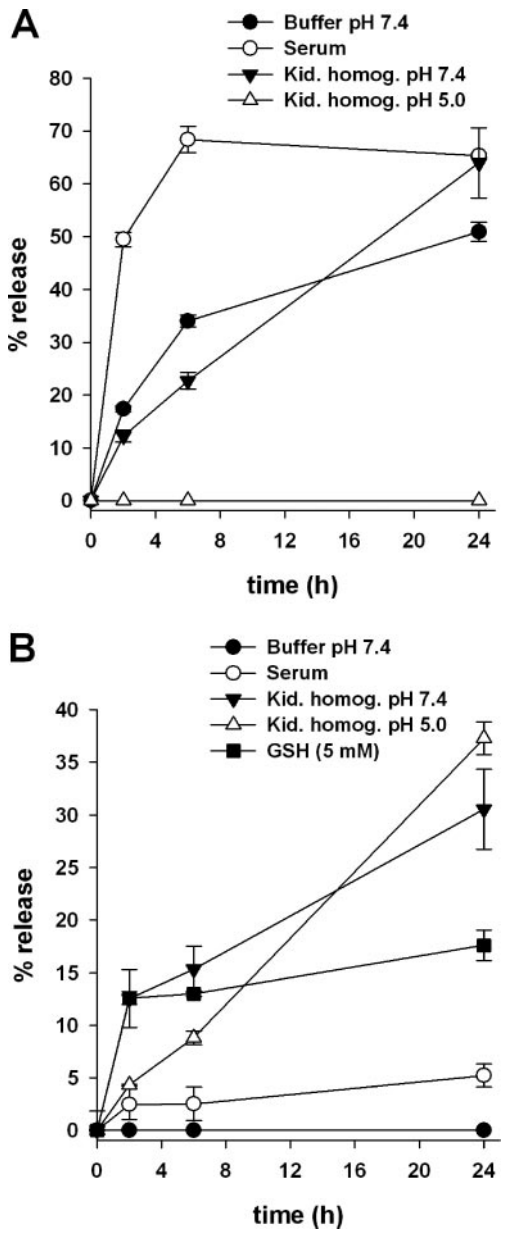

Fig. 3. Release of SB202190 from SB-carbamate-LZM (A) and SB-ULS-LZM (B) in different conditions. The experiment was performed in triplicate, mean ± S.E.M.

Toxicity of Platinum-Containing Compounds in Tubular Cells

The effect of ULS on viability of renal tubular epithelial cells (NRK-52E) was compared with an equimolar concentration of the well known cytostatic drug cisplatin. ULS showed no effect on the viability of the cells at the concentration of 100 μM, whereas cisplatin caused a significant reduction of the number of viable cells (Fig. 4A). We also tested the drug-ULS and drug-ULS-LZM constructs and found them nontoxic in comparison with their respective controls (Fig. 4, B and C).

Pharmacokinetics of SB-ULS-LZM Conjugate

In prior studies with other drug-LZM conjugates, we observed a rapid renal accumulation of these products after i.v. administration (Prakash et al., 2005b). We used this knowl-

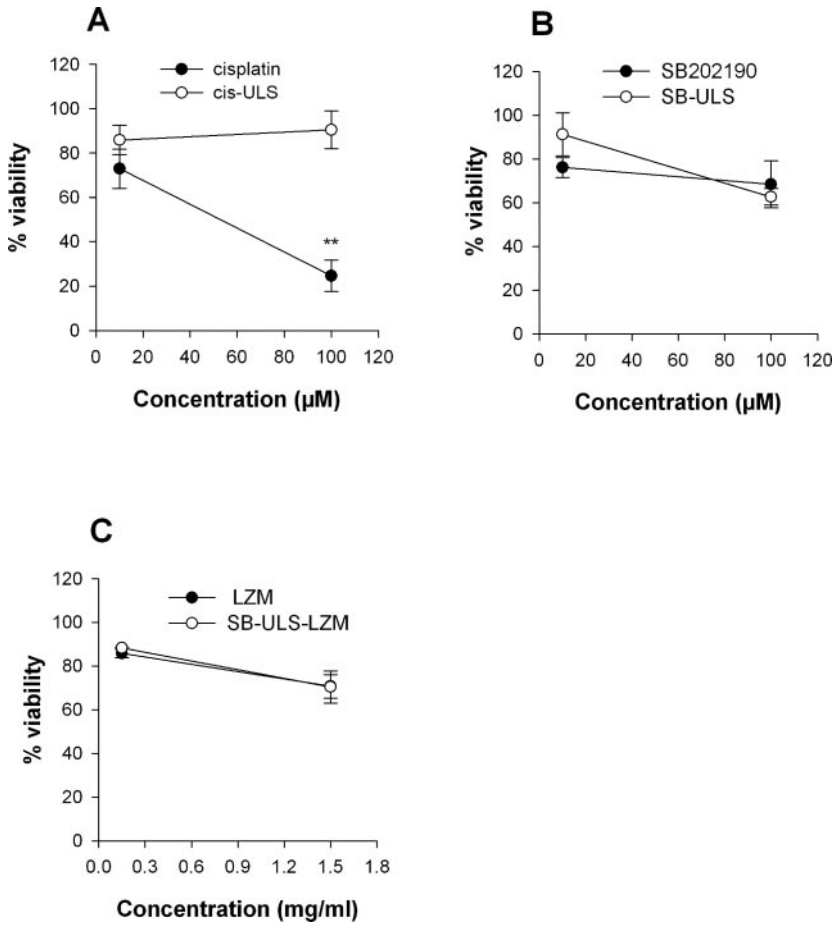

Fig. 4. Comparison of cellular toxicity of different platinum containing compounds on renal tubular cells (NRK-52E). Cells were incubated for 24 h with indicated compounds, after which cell viability was determined by the Alamar blue assay. Concentrations tested corresponded to 10 and 100 μM platinum or were equivalent to the amount of drug (SB202190) or protein (LZM). Data represent the mean ± S.E.M. for three independent experiments. **, $p < 0.01$.

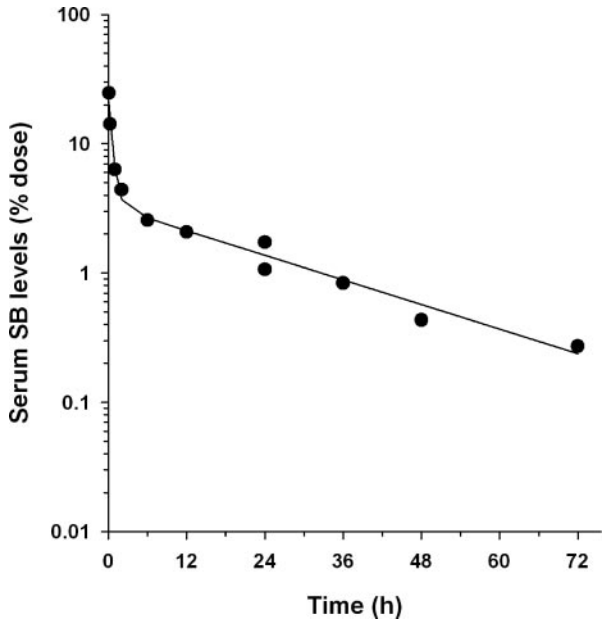

Fig. 5. Serum disappearance curve of SB-ULS-LZM. Symbols, percentage dose of SB202190 at each time point; continuous line, pharmacokinetic data-fit curve (two-compartment model).

TABLE 1

Pharmacokinetic parameters (two-compartment model) derived from serum concentration-time curves after a single i.v. dose of 16 mg/kg (equivalent to 376 μg/kg SB202190) of SB-ULS-LZM in rats

Parameters	Values (Mean ± S.E.)
V1 (ml/kg)	101 ± 18
CL_{ini} (ml/kg/h)	149 ± 28
CL (ml/kg/h)	24.0 ± 1.5
$AUC_{(0-\infty)}$ (h·μg/ml)	15.6 ± 1.0
$t_{1/2}$ α (h)	0.41 ± 0.1
$t_{1/2}$ β (h)	18.7 ± 1.8

V1, volume of central compartment; CL_{ini}, sum of elimination and distribution clearance from central compartment; CL, total serum clearance; $AUC_{(0-\infty)}$, area under the curve from zero to infinity; $t_{1/2\alpha}$, distribution half life; $t_{1/2\beta}$, elimination half life.

edge to design a protocol for the pharmacokinetic studies with SB-ULS-LZM that allowed optimal estimation of the pharmacokinetic parameters. In such a so-called optimal sampling protocol, the data are fitted to a nonlinear multicompartment model (Multifit program). The serum-disappearance curve of SB-ULS-LZM, which followed a two-compartment pharmacokinetic model, is shown in Fig. 5. Because we sacrificed the individual animals at different time points rather than at fixed moments in time, calculated parameters are less prone to extrapolation and are consequently more reliable (Table 1). Only carrier-bound SB202190 was detected in the serum, whereas free drug was absent at all time points. From this result, we concluded that the conjugate remained stable in the serum. Furthermore, in accordance with other drug-LZM conjugates, SB-ULS-LZM accumulated efficiently in the kidneys within 1 h following the i.v. injection (Fig. 6A). The accumulation of the conjugate in proximal tubular cells was confirmed by anti-LZM immunohistochemical staining on kidney sections (Fig. 6, C and D). In parallel with the accumulation of ULS-bound drug, we observed con-

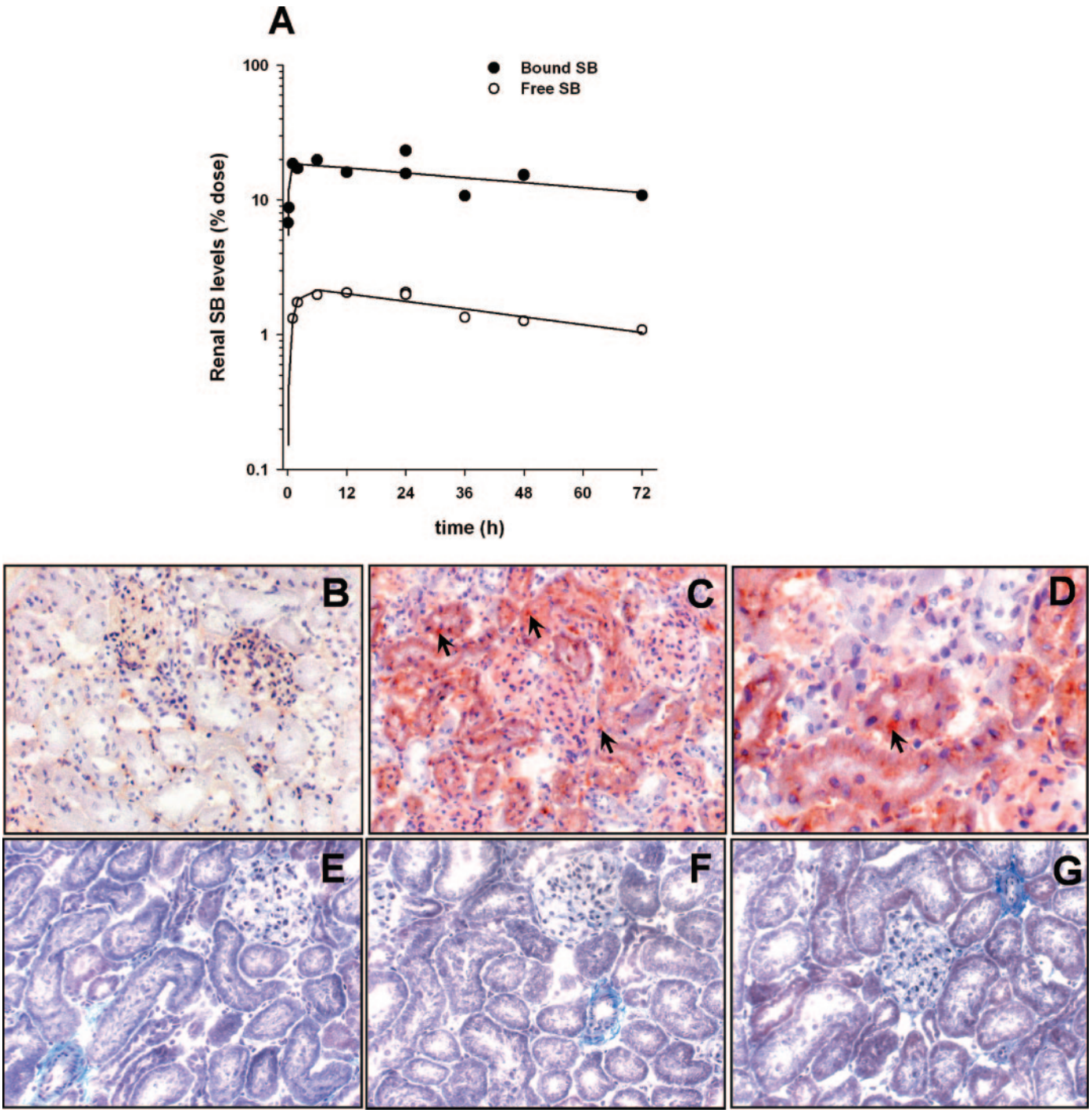

Fig. 6. Renal levels of SB-ULS-LZM (A). Symbols, percent dose of SB202190 at each time point; continuous line, pharmacokinetic data-fit curve. The curve fitting was performed with Multifit software by two-compartment model including peripheral drug levels. B to D, anti-LZM immunohistochemical staining on kidney sections. B, untreated animals; C and D, SB-ULS-LZM-treated animals at 1 h. Arrows in C and D, staining for lysozyme in tubular cells. C (magnification, 200×), accumulation of SB-ULS-LZM in kidneys, which appeared to be allocated within the tubular cells as observed at magnification 400× (D). Masson staining shows renal morphology in untreated animals (E) and SB-ULS-LZM-treated animals at 24 (F) and 72 (G) h at 200× magnification. There is no change in the morphology of the proximal tubular cells after 24 (E versus F) or 72 (E versus G) h after administration of the conjugate.

tinuous levels of free SB202190 in the kidneys at all time points starting from 1 h after dosing until the last sampling point, 3 days after injection (Fig. 6A). Prior studies in our group had demonstrated that free SB202190 does not accumulate in the kidneys upon i.v. administration (Prakash et al., 2005a). Therefore, the presence of free drug in the kidneys predominantly reflects the continuous local release of SB202190 from the conjugate within the kidneys.

Apart from serum and kidneys, we analyzed liver samples for the presence of the conjugate. Although bound drug was detectable in liver homogenates, no free drug was detected (data not shown). Furthermore, we investigated the excretion

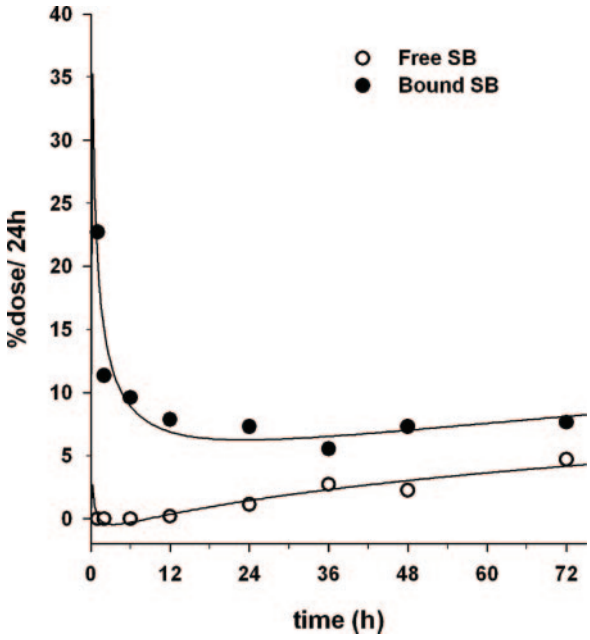

Fig. 7. Urinary excretion rate of free and linker-bound SB202190 after administering the conjugate. Symbols, percentage dose per 24 h of SB202190 at each time point; continuous line, fitted curve.

of the drug into the urine that was collected during the experimental period in metabolic cages. We observed a prolonged and continuous excretion of both free SB20190 and linker-bound drug that corresponded to the continuous release profile in the kidneys (Fig. 7).

Nephrotoxicity is one of the most prominent side effects of cisplatin treatment and is mostly associated with acute toxicity to renal tubular cells (Taguchi et al., 2005). Thus, administration of a platinum-containing compound that efficiently accumulates in the proximal tubule may induce unwanted nephrotoxicity. Therefore, we closely examined the animals during the pharmacokinetic study and observed no apparent discomfort up to 72 h. Furthermore, we determined renal function and other parameters to determine platinum-related toxicities (Table 2). Creatinine clearance remained normal in animals receiving vehicle or conjugate, whereas an increase in urinary protein levels was found with SB-ULS-LZM in comparison with untreated rats. However, the observed value of the conjugate-treated group was well within normal limits. Second, we detected tubular damage by TUNEL staining on kidney sections, which clearly demonstrated that cisplatin-treated animals had higher apoptotic tubular cells as compared with untreated rats. In contrast, SB-ULS-LZM-treated rats showed no increase in the number of apoptotic cells, despite the comparable levels of platinum in the kidneys of cisplatin and SB-ULS-LZM-treated groups. Morphological analysis of kidney sections using Masson staining showed no renal damage by SB-ULS-LZM treatment in comparison with control animals (Fig. 6, E–G). Nephrotoxicity by cisplatin treatment was furthermore associated with a loss of body weight, whereas SB-ULS-LZM treated rats showed a constant body weight during the experiment for 3 days. From these results, we concluded that the pharmacological and toxicological behavior of the linker ULS is quite different from those of the cytostatic agent cisplatin.

Effect of SB-ULS-LZM Conjugate in HK-2 Cells

The potential therapeutic effect of SB-ULS-LZM was evaluated in proximal tubular cell of human origin (HK-2 cells). Intracellular delivery of the conjugate is dependent on receptor-mediated endocytosis from the medium. However, the capability to internalize proteins is rapidly lost in many kidney cell lines, which renders the conjugate ineffective in vitro, despite its efficient intratubular accumulation in vivo. HK-2 cells are known to internalize proteins (Gudehithlu et al., 2004), whereas the NRK-52E cells described earlier in this paper did not reabsorb LZM (data not shown). After incubation for 24 h with TGF-β1, we detected a 10-fold higher gene expression for procollagen-Iα1 as compared with resting levels (Fig. 8). Treatment with SB-ULS-LZM conjugate for 48 h resulted in a significant reduction by 64% of the induced gene, as did the treatment with free SB202190 (10 μM). Treatment with the LZM carrier alone did not affect the TGF-β1-induced profibrotic signaling. From these results, we concluded that the conjugate was capable to deliver pharmacologically active drug into the designated target cells.

Effect of SB-ULS-LZM Conjugate in the I/R Rat Model

The pharmacological efficacy of SB-ULS-LZM was evaluated in the renal I/R model, which finally leads to fibrosis within a period of 1 to 4 days. Several studies have established the involvement of activated p38 in epithelial cells after I/R injury (Furuichi et al., 2002; Mehta et al., 2002) We hypothesized that a single dose of SB-ULS-LZM would afford sufficient amounts of active drug in the kidney due to its controlled drug release profile, as shown in Fig. 6A. The conjugate was administered 2 h before ischemia so that the conjugate could accumulate completely within the kidneys. First, we examined the activation of p38 MAPK in the kidney by immunostaining for p-p38-positive cells. Our results confirmed that p38 was still activated after 4 days of I/R injury as compared with sham-operated animals.

TABLE 2

Summary of the parameters to determine platinum-related nephrotoxicity in SB-ULS-LZM and cisplatin-treated animals

Data for untreated and cisplatin groups are represented as mean ± S.E.M., $n = 4$ at 24 h. The values for SB-ULS-LZM are shown as mean ± S.E.M., $n = 4$ at 24, 32, 48, and 72 h, with the exception of TUNEL-positive cells, which is $n = 5$ at 24 ($n = 2$), 32, 48, and 72 h.

Parameters	Untreated Group	SB-ULS-LZM-Treated Group	Cisplatin-Treated Group
Creatinine clearance (ml/min)	1.0 ± 0.13	0.8 ± 0.03	1.1 ± 0.13
Urinary protein levels (mg/day)	19.16 ± 1.3	29.6 ± 2.0††	23 ± 3.6
TUNEL-positive cells (numbers per field)	46.4 ± 4.14	42.7 ± 18**	187 ± 26††
Renal platinum concentration (nmol/g)	N.D.	37.0 ± 1.2**	28.4 ± 0.8
Change in body weight(%)	−1.75 ± 2.25	+0.3 ± 1.2*	−5.0 ± 0.6††

The differences between cisplatin and SB-ULS-LZM groups are: * $p < 0.05$ and ** $p < 0.01$. The differences versus untreated groups are † $p < 0.05$ and †† $p < 0.01$. N.D., not detectable.

Vehicle-treated I/R rats had dilated and damaged tubules that strongly showed p-p38-positive cells (grade, +++) in both renal cortex and medulla as compared with sham-operated animals (grade, −/+). In the cortex, neither of the treatments showed any reduction in p-p38-positive cells. However, treatment with SB-ULS-LZM reduced the number of p-p38-positive cells in the medulla (grade +, Fig. 9B), but no reduction was found in SB202190-treated animals (grade, +++; Fig. 9C).

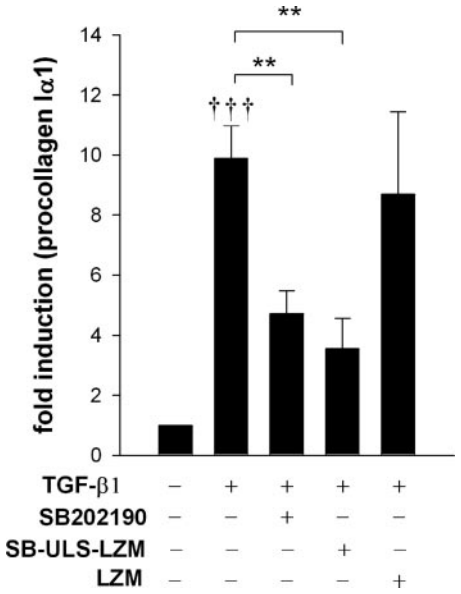

Fig. 8. Effects of SB202190 and SB-ULS-LZM on the gene expressions of procollagen-Iα1 induced by TGF-β1 in HK-2 cells. Cells were grown to 80% confluence and then deprived from serum for 24 h. The SB-ULS-LZM conjugate (SB-ULS-LZM, 155 μg/ml) or methionine-modified LZM (LZM, 155 μg/ml) was incubated at the time of serum deprivation, whereas SB202190 (10 μM) was added 1 h before adding TGF-β1 (10 ng/ml) to the cells. The cells were further cultured for 24 h. Then cells were harvested for RNA isolation. The mRNA expressions were determined by quantitative RT-PCR. Data represent the mean ± S.E.M. for at least three experiments. Differences versus control are presented as: †††, $p < 0.001$. Other differences are: **, $p < 0.01$.

Moreover, to study the effect of SB-ULS-LZM conjugate on fibrosis, we investigated the renal deposition of the fibrosis marker α-SMA by immunohistochemical analysis. We found that after 4 days of I/R injury, α-SMA expression was highly increased in the tubulointerstitial space of the renal cortex (grade, +++; Fig. 9D) in comparison with sham-operated animals (grade, −/+). A single dose of the SB-ULS-LZM conjugate reduced α-SMA expression (grade, ++; Fig. 9E), whereas nontargeted SB202190 did not affect the expression of α-SMA (grade, +++; Fig. 9F).

Discussion

Data from the present study confirm that blockade of p38 MAPK within renal tubular cells diminishes the activation of inflammatory- and fibrosis-related genes, which may be important for the treatment of renal fibrosis. We also demonstrated that we can deliver the p38 inhibitor SB202190 to proximal tubular cells in the kidney and that the conjugate has a unique slow-release profile. Moreover, after only a single dose, the targeted SB-ULS-LZM conjugate showed modest beneficial effects in renal I/R-injured rats.

Low-molecular weight proteins like LZM accumulate in the kidneys via megalin-mediated endocytosis and can be exploited as renal-specific drug carriers (Haas et al., 2002). In the present study, we describe the successful coupling of SB202190 to LZM using two different linkage strategies, either employing a carbamate bond or a coordinative bond between drug and carrier. Our in vitro stability experiments

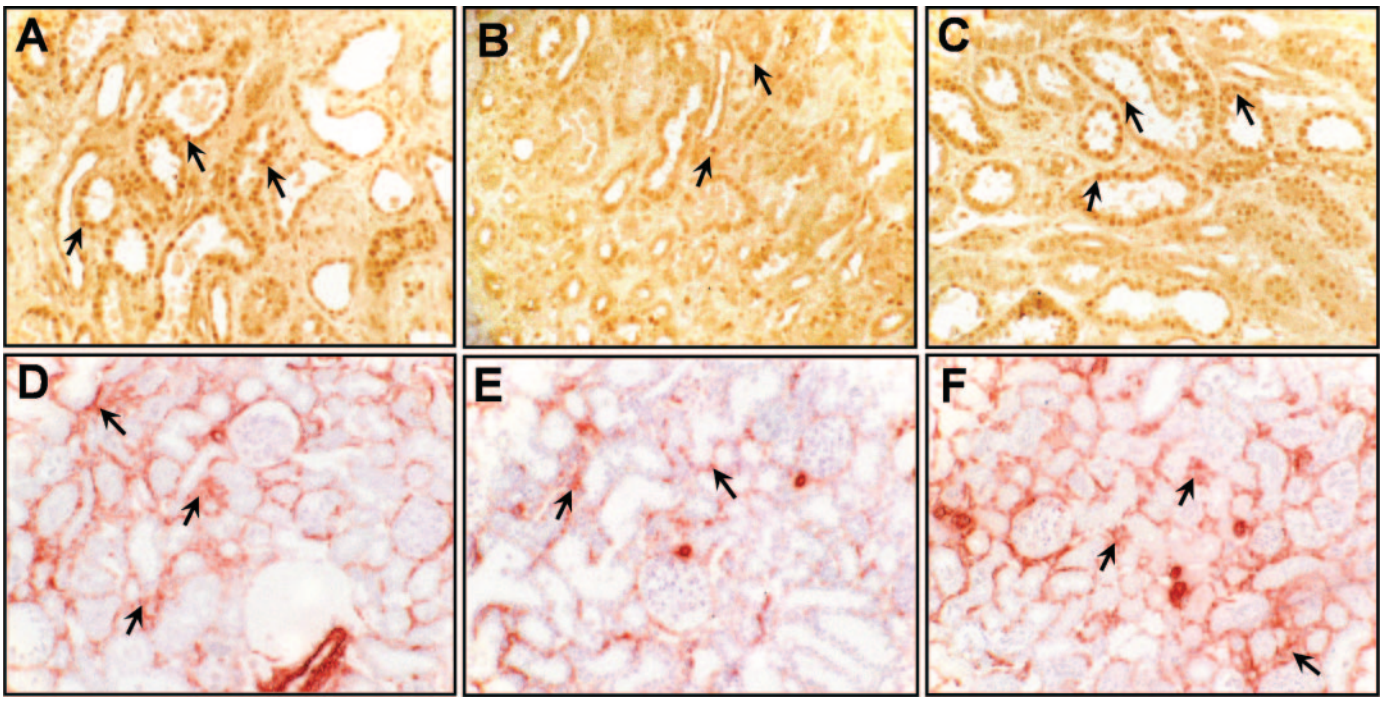

Fig. 9. Representative photomicrographs of the immunohistochemical detection of p-p38-positive cells in renal medulla (A–C; 200×) and α-SMA expression in renal cortex (D–F; 100×) 4 days after unilateral ischemia-reperfusion injury. A and D, vehicle-treated animals; B and E, SB-ULS-LZM-treated animals; C and F, SB202190-treated animals. Arrows in A to C, immunolocalization (dark-brown color) of p-p38-positive nuclei in the tubular cells corresponding to the dilated and injured tubules. Arrows in D to F, localization of α-SMA in tubulointerstitial space with red color.

demonstrated that the carbamate linkage was sensitive to serum enzymes, most probably esterases. As a consequence, free drug will be prematurely released before the SB-carbamate-LZM conjugate can reach the kidney. In contrast, the conjugate prepared with ULS displayed high stability in serum and exhibited a slow release of the drug in kidney homogenate. This slow-release phenomenon can be explained by the ligand exchange kinetics of platinum (Reedijk, 2003). Transition metals like platinum make coordination bonds with the ligands that are weaker than covalent bonds. However, the ligand exchange behavior of platinum-coordinated compounds is quite slow, which gives them a high kinetic stability (Reedijk, 2003). GSH is a likely candidate to act as an intracellular ligand (Ikeda et al., 2001). Efficient drug displacement by GSH was proven for the present SB-ULS-LZM conjugate when it was incubated at the intracellular concentration of 5 mM GSH. In addition, the drug release might also be facilitated by cellular enzymes since kidney homogenates at pH 7.4 containing cytosolic active enzymes or at pH 5 at which lysosomal enzymes are active released SB202190 from SB-ULS-LZM. Among others, lysosomal degradation of the LZM protein, which generates methionine and cysteine residues, may facilitate drug release. Other enzymes that may favor intracellular drug release are glutathione generation enzymes like thioredoxin and glutathione reductases. Based on stability and release characteristics that were favorable for SB-ULS-LZM compared with SB-carbamate-LZM, we pursued our studies with SB-ULS-LZM.

Although platinum-containing compounds such as cisplatin are considered nephrotoxic (Wolfgang et al., 1994; Park et al., 2002), ULS or SB-ULS constructs did not produce any toxicity to NRK-52E renal tubular cells even at high (100 μM) concentrations. Moreover, in vivo treatment with the SB-ULS-LZM conjugate did not produce any toxicity because there was no effect on renal function, renal morphology, and body weight until 72 h. In addition, no increase in the number of apoptotic cells was observed, indicating the safety of SB-ULS-LZM conjugate to the kidneys.

The pharmacokinetic study indicated that SB-ULS-LZM was quickly removed from the general circulation and subsequently slowly eliminated from the renal tissue. The localization of the carrier protein in the tubular cells detected by anti-LZM staining confirms that the conjugate was reabsorbed in the tubular cells. Within these cells, the free drug was released from the conjugate almost at a constant rate for 72 h and subsequently excreted in urine. Since we found both free and linker-bound drug in the urine, it is apparent that a part of SB-ULS-LZM was not completely converted to the free drug. This suggests that the carrier protein in the conjugate was degraded by the lysosomal enzymes and released in the form of various products SB-ULS-X, in which X represents a thiol compound like methionine or any other moiety that can bind to platinum. Subsequently, SB-ULS-X released free SB202190, which was excreted in the urine and detected as a free drug, or SB-ULS-X might be eliminated by tubular cells intactly into the urine.

Our in vitro incubation of tubular cells with SB202190 demonstrated a reduction in the gene expressions of MCP-1, procollagen-Iα1, and TIMP-1, either induced by BSA or TGF-β1. These genes are highly relevant because they are upregulated during renal fibrosis as demonstrated by many studies (Lloyd et al., 1997; Duymelinck et al., 2000; Grygielko et al., 2005). The effect of SB202190 on albumin-induced fibrotic markers was less strong than at TGF-β1-induced genes. This may be explained by the nature of albumin-induced gene expression in tubular cells, which causes the activation of several other signaling pathways apart from p38 MAPK (Burton et al., 1999; Yard et al., 2001). We examined the activity of the SB-ULS-LZM conjugate in HK-2 cells that are known for their capacity to internalize proteins via endocytosis (Gudehithlu et al., 2004). Incubation of the HK-2 cells with TGF-β1 activated profibrotic signaling, which was substantially (64%) reduced by preincubation with the SB-ULS-LZM conjugate. Because our in vitro stability studies had demonstrated that less than 10% of the coupled drug was released in the cell culture medium, such an effect can only be effectuated after internalization and processing of the conjugate into active drug.

We examined the efficacy of SB-ULS-LZM after renal I/R injury because p38 is activated in renal tubular cells after ischemia (Furuichi et al., 2002; Mehta et al., 2002), and I/R injury finally leads to fibrosis (Jain et al., 2000). Our data on p-p38 staining confirmed that p38 is still activated in tubular cells 4 days after I/R injury and p-p38-positive cells were well correlated with the injured tubules. Furthermore, we demonstrated that a single dose of SB-ULS-LZM was capable of lowering p38 activation, which is in line with the continuous levels of free drug. A reduction in p-p38-positive cells was only found in the renal medulla but not in the cortex, which is the primary site of proximal tubular cells. Either SB202190 was released from the conjugate, redistributed from the cortical tubular cells to the medulla, and exerted the effect over there, or the effect in the cortex was not visualized due to the very high activation of p38 in the cortex. Most probably, the latter is the case because the expression of the fibrosis marker α-SMA in the cortex was reduced. In contrast to SB-ULS-LZM, nondelivered SB202190 did not affect the expression of either p-p38 or α-SMA, presumably because the free drug is rapidly eliminated from the body and does not reach the kidney in high levels during the 4-day period. Because we have administered similar amounts of SB202190 in either treatment group, we can attribute the improved efficacy of SB202190 to its renal delivery. However, further studies are needed to elucidate the mechanism of action of the conjugate and how p38 activation in different cell types is involved.

We conclude that p38 MAPK inhibition in proximal tubular cells is in potential an interesting approach to treat renal fibrosis. Such a strategy involves the development of a renal-specific conjugate that can successfully deliver p38 MAPK inhibitors to the renal tubular in the kidney. Our new linkage technology ULS produced drug-LZM conjugates that display a sustained release of the drug in tubular cells for several days, which is an advantageous characteristic for drugs against chronic diseases. In addition, a large number of drugs containing nitroaromatic rings such as pyridine, pyrimidine, or imidazole groups (English and Cobb, 2002; Laufer and Wagner, 2002) may be potential candidates for the ULS coupling approach.

Acknowledgments

We thank Annemiek van Loenen-Weemaes for technical assistance in performing animal experiments and Annie van Dam and Margot Jeronimus-Stratingh (Department of Analytical Biochemis-

try, University of Groningen) for assistance in mass spectrometry analysis. Colleagues at Kreatech are acknowledged for critical reading of the manuscript.

References

Bhaskaran M, Reddy K, Radhakrishanan N, Franki N, Ding G, and Singhal PC (2003) Angiotensin II induces apoptosis in renal proximal tubular cells. *Am J Physiol* **284:**F955–F965.

Burton CJ, Combe C, Walls J, and Harris KP (1999) Secretion of chemokines and cytokines by human tubular epithelial cells in response to proteins. *Nephrol Dial Transplant* **14:**2628–2633.

de Borst MH, Wassef L, Kelly DJ, van Goor H, and Navis G (2005) Mitogen activated protein kinase signaling in the kidney: target for intervention? *Signal Transduction* **5:**1–22.

Duymelinck C, Dauwe SE, De Greef KE, Ysebaert DK, Verpooten GA, and De Broe ME (2000) TIMP-1 gene expression and PAI-1 antigen after unilateral ureteral obstruction in the adult male rat. *Kidney Int* **58:**1186–1201.

English JM and Cobb MH (2002) Pharmacological inhibitors of MAPK pathways. *Trends Pharmacol Sci* **23:**40–45.

Furuichi K, Wada T, Iwata Y, Sakai N, Yoshimoto K, Kobayashi KK, Mukaida N, Matsushima K, and Yokoyama H (2002) Administration of FR167653, a new anti-inflammatory compound, prevents renal ischaemia/reperfusion injury in mice. *Nephrol Dial Transplant* **17:**399–407.

Gonzalo T, Talman EG, van de Ven A, Temming K, Greupink R, Beljaars L, Reker-Smit C, Meijer DK, Molema G, Poelstra K, et al. (2006) Selective targeting of pentoxifylline to hepatic stellate cells using a novel platinum-based linker technology. *J Control Release* **111:**193–203.

Grygielko ET, Martin WM, Tweed C, Thornton P, Harling J, Brooks DP, and Laping NJ (2005) Inhibition of gene markers of fibrosis with a novel inhibitor of transforming growth factor-beta type I receptor kinase in puromycin-induced nephritis. *J Pharmacol Exp Ther* **313:**943–951.

Gudehithlu KP, Pegoraro AA, Dunea G, Arruda JA, and Singh AK (2004) Degradation of albumin by the renal proximal tubule cells and the subsequent fate of its fragments. *Kidney Int* **65:**2113–2122.

Haas M, Moolenaar F, Meijer DKF, and De Zeeuw D (2002) Specific drug delivery to the kidney. *Cardiovasc Drugs Ther* **16:**489–496.

Harrison EM, McNally SJ, Devey L, Garden OJ, Ross JA, and Wigmore SJ (2006) Insulin induces heme oxygenase-1 through the phosphatidylinositol 3-kinase/Akt pathway and the Nrf2 transcription factor in renal cells. *FEBS J* **273:**2345–2356.

Ikeda K, Miura K, Himeno S, Imura N, and Naganuma A (2001) Glutathione content is correlated with the sensitivity of lines of PC12 cells to cisplatin without a corresponding change in the accumulation of platinum. *Mol Cell Biochem* **219:**51–56.

Jain S, Bicknell GR, and Nicholson ML (2000) Molecular changes in extracellular matrix turnover after renal ischaemia-reperfusion injury. *Br J Surg* **87:**1188–1192.

Koshikawa M, Mukoyama M, Mori K, Suganami T, Sawai K, Yoshioka T, Nagae T, Yokoi H, Kawachi H, Shimizu F, et al. (2005) Role of p38 mitogen-activated protein kinase activation in podocyte injury and proteinuria in experimental nephrotic syndrome. *J Am Soc Nephrol* **16:**2690–2701.

Kumar S, Boehm J, and Lee JC (2003) p38 MAP kinases: key signalling molecules as therapeutic targets for inflammatory diseases. *Nat Rev Drug Discov* **2:**717–726.

Laufer SA and Wagner GK (2002) From imidazoles to pyrimidines: new inhibitors of cytokine release. *J Med Chem* **45:**2733–2740.

Lloyd CM, Minto AW, Dorf ME, Proudfoot A, Wells TN, Salant DJ, and Gutierrez-Ramos JC (1997) RANTES and monocyte chemoattractant protein-1 (MCP-1) play an important role in the inflammatory phase of crescentic nephritis, but only MCP-1 is involved in crescent formation and interstitial fibrosis. *J Exp Med* **185:**1371–1380.

Meguid El NA and Bello AK (2005) Chronic kidney disease: the global challenge. *Lancet* **365:**331–340.

Mehta A, Sekhon CP, Giri S, Orak JK, and Singh AK (2002) Attenuation of ischemia/reperfusion induced MAP kinases by *N*-acetyl cysteine, sodium nitroprusside and phosphoramidon. *Mol Cell Biochem* **240:**19–29.

Morigi M, Macconi D, Zoja C, Donadelli R, Buelli S, Zanchi C, Ghilardi M, and Remuzzi G (2002) Protein overload-induced NF-kappaB activation in proximal tubular cells requires H(2)O(2) through a PKC-dependent pathway. *J Am Soc Nephrol* **13:**1179–1189.

Park MS, De LM, and Devarajan P (2002) Cisplatin induces apoptosis in LLC-PK1 cells via activation of mitochondrial pathways. *J Am Soc Nephrol* **13:**858–865.

Prakash J, Saluja V, Visser J, Moolenaar F, Meijer DKF, Poelstra K, and Kok RJ (2005a) Bioanalysis and pharmacokinetics of the p38 MAPkinase inhibitor SB202190 in rats. *J Chromatogr B* **826:**220–225.

Prakash J, van Loenen-Weemaes AM, Haas M, Proost JH, Meijer DK, Moolenaar F, Poelstra K, and Kok RJ (2005b) Renal-selective delivery and Angiotensin-converting enzyme inhibition by subcutaneously administered captopril-lysozyme. *Drug Metab Dispos* **33:**683–688.

Reedijk J (2003) New clues for platinum antitumor chemistry: kinetically controlled metal binding to DNA. *Proc Natl Acad Sci USA* **100:**3611–3616.

Stambe C, Atkins RC, Tesch GH, Masaki T, Schreiner GF, and Nikolic-Paterson DJ (2004) The role of p38alpha mitogen-activated protein kinase activation in renal fibrosis. *J Am Soc Nephrol* **15:**370–379.

Strutz F (2001) The role of the tubular epithelial cell in renal fibrogenesis. *Clin Exp Nephrol* 62–74.

Taguchi T, Nazneen A, Abid MR, and Razzaque MS (2005) Cisplatin-associated nephrotoxicity and pathological events. *Contrib Nephrol* **148:**107–121.

Takaya K, Koya D, Isono M, Sugimoto T, Sugaya T, Kashiwagi A, and Haneda M (2003) Involvement of ERK pathway in albumin-induced MCP-1 expression in mouse proximal tubular cells. *Am J Physiol* **284:**F1037–F1045.

Wolf G, Schroeder R, Ziyadeh FN, and Stahl RA (2004) Albumin up-regulates the type II transforming growth factor-beta receptor in cultured proximal tubular cells. *Kidney Int* **66:**1849–1858.

Wolfgang GH, Dominick MA, Walsh KM, Hoeschele JD, and Pegg DG (1994) Comparative nephrotoxicity of a novel platinum compound, cisplatin, and carboplatin in male Wistar rats. *Fund Appl Toxicol* **22:**73–79.

Yard BA, Chorianopoulos E, Herr D, and van der Woude FJ (2001) Regulation of endothelin-1 and transforming growth factor-beta1 production in cultured proximal tubular cells by albumin and heparan sulphate glycosaminoglycans. *Nephrol Dial Transplant* **16:**1769–1775.

Zoja C, Donadelli R, Colleoni S, Figliuzzi M, Bonazzola S, Morigi M, and Remuzzi G (1998) Protein overload stimulates RANTES production by proximal tubular cells depending on NF-kappa B activation. *Kidney Int* **53:**1608–1615.

Address correspondence to: Dr. Robbert J. Kock, Department of Pharmaceutics, Utrecht University, Sorbonnelaan 16, 3584 CA Utrecht, The Netherlands. E-mail: R.J.Kok@pharm.uu.nl